HETE OBSERVATIONS OF THE GAMMA-RAY BURST GRB 030329: EVIDENCE FOR AN UNDERLYING SOFT X-RAY COMPONENT

R. VANDERSPEK,[1] T. SAKAMOTO,[2,3,4] C. BARRAUD,[5] T. TAMAGAWA,[3] C. GRAZIANI,[6] M. SUZUKI,[2] Y. SHIRASAKI,[3,7] G. PRIGOZHIN,[1]
J. VILLASENOR,[1] J. G. JERNIGAN,[8] G. B. CREW,[1] J.-L. ATTEIA,[5] K. HURLEY,[8] N. KAWAI,[2,3] D. Q. LAMB,[6] G. R. RICKER,[1]
S. E. WOOSLEY,[9] N. BUTLER,[1] J. P. DOTY,[1] A. DULLIGHAN,[1] T. Q. DONAGHY,[6] E. E. FENIMORE,[4] M. GALASSI,[4]
M. MATSUOKA,[10] K. TAKAGISHI,[11] K. TORII,[3,12] A. YOSHIDA,[3,13] M. BOER,[5] J.-P. DEZALAY,[14]
J.-F. OLIVE,[14] J. BRAGA,[15] R. MANCHANDA,[16] AND G. PIZZICHINI[17]

ABSTRACT

An exceptionally intense gamma-ray burst, GRB 030329, was detected and localized by the instruments on board the *High Energy Transient Explorer* satellite (*HETE*) at 11:37:14 UT on 2003 March 29. The burst consisted of two ~10 s pulses of roughly equal brightness and an X-ray tail lasting more than 100 s. The energy fluence in the 30–400 keV energy band was $S_\gamma = 1.2 \times 10^{-4}$ ergs cm^{-2}, making GRB 030329 one of the brightest GRBs ever detected. Communication of a 2′ error box 73 minutes after the burst allowed the rapid detection of a counterpart in the optical, X-ray, and radio and the ensuing discovery of a supernova with most unusual characteristics. Analyses of the burst light curves reveal the presence of a distinct, bright, soft X-ray component underlying the main GRB; the 2–10 keV fluence of this component is $\sim 7 \times 10^{-6}$ ergs cm^{-2}. The main pulses of GRB 030329 were preceded by two soft, faint, nonthermal bumps. We present details of the *HETE* observations of GRB 030329.

Subject headings: gamma rays: bursts — X-rays: individual (GRB 030329)

1. INTRODUCTION

On 2003 March 29 the *High Energy Transient Explorer* (*HETE*; Ricker et al. 2003) detected one of the brightest gamma-ray bursts (GRBs) ever recorded, GRB 030329. The intense flux of this burst and the special characteristics of the *HETE* mission allowed the 2′ localization of the burst to be

[1] Center for Space Research, Massachusetts Institute of Technology, 70 Vassar Street, Cambridge, MA 02139.

[2] Department of Physics, Tokyo Institute of Technology, 2-12-1 Ookayama, Meguro-ku, Tokyo 152-8551, Japan.

[3] RIKEN (Institute of Physical and Chemical Research), 2-1 Hirosawa, Wako, Saitama 351-0198, Japan.

[4] Los Alamos National Laboratory, P.O. Box 1663, Los Alamos, NM 87545.

[5] Laboratoire d'Astrophysique, Observatoire Midi-Pyrénées, 14 Avenue Edouard Belin, 31400 Toulouse, France.

[6] Department of Astronomy and Astrophysics, University of Chicago, 5640 South Ellis Avenue, Chicago, IL 60637.

[7] National Astronomical Observatory, Osawa 2-21-1, Mitaka, Tokyo 181-8588, Japan.

[8] Space Sciences Laboratory, University of California, Berkeley, CA, 94720-7450.

[9] Department of Astronomy and Astrophysics, University of California at Santa Cruz, 477 Clark Kerr Hall, Santa Cruz, CA 95064.

[10] Tsukuba Space Center, National Space Development Agency of Japan, Tsukuba, Ibaraki 305-8505, Japan.

[11] Faculty of Engineering, Miyazaki University, Gakuen Kibanadai Nishi, Miyazaki 889-2192, Japan.

[12] Department of Earth and Space Science, Graduate School of Science, Osaka University, 1-1 Machikaneyama-cho, Toyonaka, Osaka 560-0043, Japan.

[13] Department of Physics, Aoyama Gakuin University, Chitosedai 6-16-1 Setagaya-ku, Tokyo 157-8572, Japan.

[14] Centre d'Etude Spatiale des Rayonnements, Observatoire Midi-Pyrénées, 9 Avenue de Colonel Roche, 31028 Toulouse Cedex 4, France.

[15] Instituto Nacional de Pesquisas Espaciais, Avenida Dos Astronautas 1758, São José dos Campos 12227-010, Brazil.

[16] Department of Astronomy and Astrophysics, Tata Institute of Fundamental Research, Homi Bhabha Road, Mumbai 400 005, India.

[17] Consiglio Nazionale delle Ricerche, IASF, Sezione di Bologna, via Piero Gobetti 101, 40129 Bologna, Italy.

communicated worldwide 72 minutes after the onset of the burst. This led, in turn, to the rapid discovery of optical, X-ray, and radio counterparts to the burst and, about one week later, to the discovery of one of the most energetic, unusual supernovae ever observed, SN 2003dh (Stanek et al. 2003; Hjorth et al. 2003). This watershed event showed conclusively that at least some long GRBs occur in conjunction with supernovae. Such an association was predicted by the collapsar model (Woosley 1993; MacFadyen & Woosley 1999).

The instruments on *HETE* allow the study of prompt radiation down to energies as low as 2 keV. The combination of high flux and low-energy sensitivity has allowed us to carry out very detailed analyses of the prompt emission of GRB 030329. These analyses have revealed soft features in the light curve: faint, nonthermal, soft X-ray "bumps" before the main GRB and a bright, soft X-ray component underlying the main GRB. In this paper, we describe the *HETE* observations of the prompt emission of GRB 030329.

2. DISCOVERY

GRB 030329 was detected by the *HETE* satellite (Ricker et al. 2003) as trigger H2652 at 11:37:14.7 UT (41,834.7 SOD) on 2003 March 29 (Vanderspek et al. 2003). GRB 030329 was seen as a very bright double-pulsed burst with a duration of over 100 s in all three *HETE* instruments: Fregate (7–400 keV; Atteia et al. 2003), the Wide-Field X-Ray Monitor (WXM, 2–25 keV; Shirasaki et al. 2003), and the Soft X-Ray Camera (SXC, 2–10 keV; Villasenor et al. 2003). GRB 030329 had a 30–400 keV fluence of $S_\gamma = 1.18 \times 10^{-4}$ ergs cm^{-2}, making it one of the brightest GRBs detected by *HETE* to date and placing it among the top 1% of the brightest GRBs ever detected. The burst duration was $t_{90} = 22.9$ s at high energies (30–400 keV), increasing to $t_{90} \approx 38$ s at low energies (2–10 keV); a soft X-ray tail is seen extending more than 100 s after burst onset.

The burst was localized by the SXC to a 2′ radius error circle (90%) centered at $\alpha = 10^\text{h}44^\text{m}49^\text{s}$, $\delta = +21°28'44''$ (J2000);

this position was distributed to the GRB Coordinates Distribution Network (GCN) 73 minutes after the burst. Torii (2003) began optical observations of the SXC error region less than 2 minutes after the distribution of the GCN Notice, Peterson & Price (2003) 15 minutes later; both observations revealed a bright ($R < 13$) optical transient (OT) just outside the SXC error circle. The bright OT was monitored by many observers over the following days (Uemura 2003; Smith et al. 2003; Gal-Yam et al. 2003; Klose et al. 2003; Burenin et al. 2003; Lipunov et al. 2003; Price et al. 2003). Greiner et al. (2003) reported a redshift of 0.1685, making GRB 030329 the closest GRB with a measured redshift after GRB 980425 (Lidman et al. 1998; Tinney et al. 1998) and GRB 031203 (Prochaska et al. 2003; Watson et al. 2004). The emergence of the signature of a Type Ic supernova from the spectrum of the optical counterpart (Matheson et al. 2003; Stanek et al. 2003; Hjorth et al. 2003) solidifies the association of some GRBs with core-collapse supernovae.

Prompt follow-up observations revealed the enormous brightness of GRB 030329 at other wavelengths. An *RXTE* observation of the X-ray afterglow starting less than 5 hr after the burst revealed the source to have a 2–10 keV flux of 1.4×10^{-10} ergs cm^{-2} s^{-1}, one of the brightest GRB X-ray afterglows ever measured (Marshall & Swank 2003). VLA observations at 8.46 GHz 14 hr after the burst (Berger et al. 2003) revealed a 3.5 mJy source, the brightest radio afterglow yet measured. The brightness of the radio afterglow was confirmed in the days following the burst at a wide range of radio wavelengths (Pooley 2003; Pramesh Rao et al. 2003; Hoge et al. 2003; Kuno et al. 2003; Finkelstein et al. 2003). GRB 030329 was also detected as a sudden ionospheric disturbance (Schnoor et al. 2003), as the incoming X-ray flux was sufficiently strong to create a global surge in the electron density on the illuminated side of the Earth.

3. OBSERVATIONS

GRB 030329 was detected by Fregate as an 8.3 σ excess in the 7–80 keV band on the 1.3 s timescale trigger. This excess was due to a soft, relatively weak precursor; 13 s later, the burst was as bright as any seen during the *HETE* mission. Real-time reports of the burst brightness via the *HETE* VHF system (Crew et al. 2003) showed the significance of the burst in the WXM exceeding the 7 bits allotted in the telemetry stream at signal-to-noise ratio S/N = 127. At the same time, the image S/N reported from the WXM was 60, twice that of the previous brightest burst (GRB 020813).

Ground analyses of the downlinked data starting ∼40 minutes after the trigger confirmed the magnitude of the burst. The burst was detected at a S/N of over 300 in both Fregate and the WXM, and over 100 in the SXC; this burst is the brightest *HETE* has detected in the 7–80 keV band. Unfortunately, the burst was *so* bright and *so* long that the Fregate flight software decided the burst was due to an increase in the overall background rate and "invalidated" the burst in flight. As a result, the initial real-time GCN messages indicated that H2652 was *not* a real GRB. More important, however, is the fact that time-tagged photons are not downlinked from the Fregate instrument for bursts that are invalidated in flight.[18] The temporal

---

[18] This same scenario occurred 24 hr earlier on the bright burst GRB 030328 (H2650), the only two times in the course of the *HETE* mission that real GRBs have been invalidated in flight. The flight software has since been modified to prevent bright bursts from being invalidated.
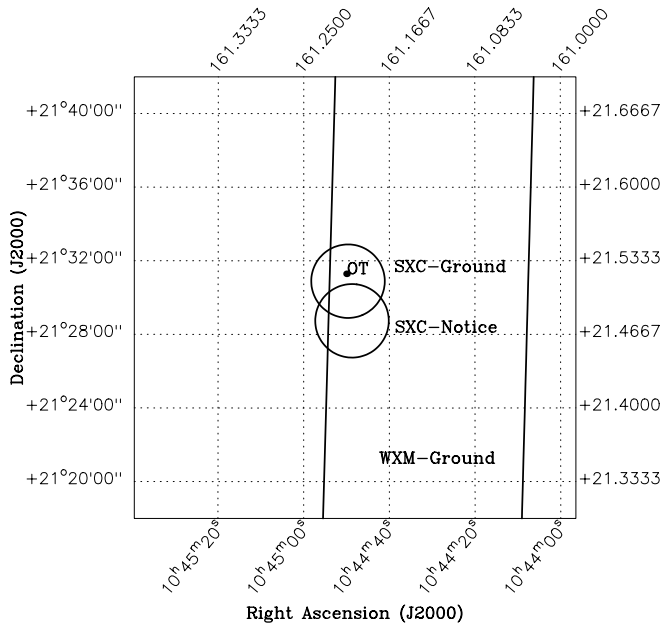
and spectral analyses of Fregate data were therefore done with survey data: light curves in three broad energy bands (band A, 7–40 keV; band B, 7–80 keV; and band C, 30–400 keV) at 80 ms time resolution and 128 channel spectral data products with a time resolution of 5.2 s.

3.1. *Localization*

GRB 030329 was very bright in X-rays; the burst was detected at a S/N of 350 in the WXM. However, the large incident angle of the burst was such that only one of the two X detectors and one of the two Y detectors of the WXM were illuminated. Unfortunately, the Y detector illuminated by the burst was YB, which was lost to a micrometeorite impact in 2003 January; as a result, while the WXM could be used to determine the X position very precisely, the Y position could only be crudely determined, based on the relative illumination of the six wires in the X detectors. Fortunately, despite the large incident angle, GRB 030329 was well detected in both the SXC X and Y detectors.

The real-time localization of GRB 030329 calculated in flight reflected these facts; the image S/N calculated on board (which reflects the strength of the peak in the cross-correlation map) was 60 in X, but less than 2 in the Y direction. As the SXC flight imaging software, which looks for significant cross-correlation peaks near the WXM localization, requires image S/N values greater than 3 in both WXM axes to proceed, no real-time SXC localization was available.

Ground analyses of the WXM and SXC data began after the full data set was downlinked, at 12:10 UT (33 minutes after the burst). It quickly became clear that only the X detector was illuminated, limiting the WXM localization to a box measuring $12' \times 2\overset{\circ}{.}25$. Fortunately, the burst was so bright in the SXC that it was possible to calculate a position without reference to the WXM position, and the SXC position was in the WXM error box. The SXC localization was distributed by GCN Notice at 12:50 UT (73 minutes after the burst) as a $2'$ circle centered on $\alpha = 10^h 44^m 49^s$, $\delta = +21°28'44''$ (J2000). Continued analyses of the SXC data after the distribution of the first GCN Notice revealed that a correction to the localization to account for systematic errors at large incident angles had not been applied, and that the procedure to distribute such localizations with a larger quoted error circles had not been followed. A revised error region that compensates for the systematic error was distributed in Vanderspek et al. (2003); it is a $2'$ circle centered on $\alpha = 10^h 44^m 50^s$, $\delta = +21°30'54''$ (J2000). The sky map of GRB 030329, showing the WXM and SXC localizations and the OT, is given in Figure 1.

GRB 030329 was observed by every spacecraft in the Interplanetary Network (IPN; *Ulysses*, *Konus-Wind*, *Mars Odyssey* [HEND and GRS], *RHESSI*, and *INTEGRAL* [SPI-ACS]), and the resulting IPN localization is fully consistent with, but does not constrain, the WXM and SXC localizations (K. Hurley 2003, private communication).

3.2. *Temporal Properties*

As shown in Figure 2, the time profile of GRB 030329 is dominated by two strong pulses separated by 11 s and an extended soft tail that continues more than 60 s after the trigger. The Fregate band D ($E > 400$ keV) light curve shows a ∼6 σ enhancement over background during the first pulse and a single 80 ms bin "spike" at $t = 26.2$ s, coincident with the peak of the second pulse. The burst duration was $t_{90} = 22.9$ s at high energies (30–400 keV), increasing to $t_{90} \approx 38$ s at low energies

Fig. 1.—Localization history of GRB 030329. Shown are a portion of the $12' \times 2°25$ WXM error region, the first SXC position (SXC-Notice), the SXC position corrected for the large systematic error at this burst's incident angle (SXC-Ground), and the location of the OT. The SXC error regions are $2'$ in radius (90%).

$(2-10 \text{ keV})$; Table 1 gives the T_{50} and T_{90} durations for various SXC, WXM, and FREGATE energy bands (Kouveliotou et al. 1993). Both duration measures decrease with increasing energy; this behavior is typical of many long-duration GRBs (Fenimore et al. 1995).

There is clear spectral evolution during the burst, as the relative brightness of the first pulse to the second pulse is larger in Fregate band C than in band A. There is also distinctly different spectral behavior in the two pulses. In Figure 3, we overlay the SXC $(2-10 \text{ keV})$ and Fregate band C light curves; while the onset of the second pulse is essentially simultaneous in all energy bands, there is a delay in the peak of the first pulse of ~ 5 s between photons with $E > 25$ keV and those with $E < 10$ keV. The nature of this evolution is discussed in more detail in § 4.1.

The inset figures of Figure 2 reveal two small precursor bumps, seen primarily in Fregate bands A and B. (The second bump in band B is in fact the trigger for this burst in Fregate.) While the bumps are not as significant in the WXM and SXC light curves, localization analyses of both WXM and SXC data show that the photons came from the same celestial coordinates as the photons from the two main pulses; this result holds for photons detected as early as $t = -13$ s. Integrating a pair of Gaussians fitted to the two bumps shows that the total of counts in the two bumps is roughly 1% of the total in the two main pulses in both bands A and B. In each bump, the $7-30$ keV counts fluence is $\sim 90\%$ of the $7-80$ keV counts fluence, indicating that the bulk of the precursor emission is less than 30 keV; the fact that the second bump is slightly more prominent than the first one in band C (see the inset of Fig. 2b) may indicate that the second bump is somewhat harder than the first. Also visible in the inset figures in Figure 2 is a general rise in the count rates at lower energies in the period leading up to the first major pulse. The burst begins in the $30-400$ keV band at $t \approx -4$ s, while $2-25$ keV photons are first detected at $t \approx -13$ s.
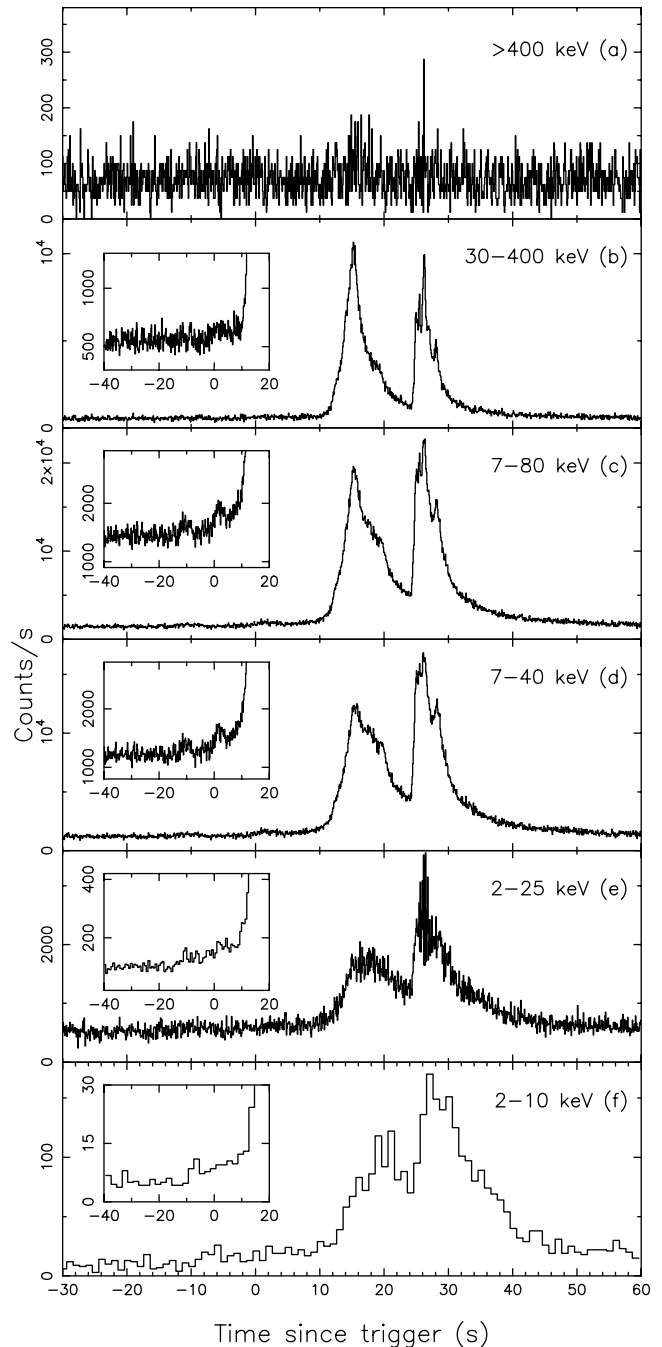

Fig. 2.—Time histories of GRB 030329. Shown are the light curves in (a) Fregate band D, (b) Fregate band C, (c) Fregate band B, (d) Fregate band A, (e) the WXM, and (f) the SXC. The inset figures show more detail for the burst precursors in each band. The time resolution of the Fregate plots is 80 ms (160 ms in the insets); for the WXM, it is 80 ms (640 ms); for the SXC, it is 1 s (2 s). The broad time bands may hide significant spectral evolution at the start of the second pulse; the short spike in band D at $t = 26.2$ s indicates that the burst was harder for a brief period at the start of the second pulse.

GRB 030329 also has a soft X-ray tail, which continues more than 100 s after the trigger. T. Tamagawa et al. (2003, private communication) have shown that an extrapolation of the $2-10$ keV photon energy flux of the afterglow (Tiengo et al. 2003; Marshall et al. 2003) back to $t = 100$ s is consistent with the $2-10$ keV photon energy flux observed in the X-ray tail at that time; the spectral index of the tail (~ -2.1) is also consistent with that cited in Tiengo et al. (2003). The soft X-ray tail

TABLE 1
Temporal Properties of GRB 030329

Instrument	Energy (keV)	T_{50} (s)	T_{90} (s)
HETE SXC	2–10	12.2 ± 0.3	34.7 ± 1.5
HETE WXM	2–25	12.8 ± 0.2	41.6 ± 0.8
	2–5	14.5 ± 0.4	52.1 ± 1.2
	5–10	12.4 ± 0.3	39.8 ± 1.0
	10–25	11.5 ± 0.2	36.9 ± 1.1
HETE FREGATE..............	7–40	11.2 ± 0.06	29.1 ± 0.6
	30–400	11.2 ± 0.05	22.8 ± 0.5

Note.—Errors are 1 σ; the SXC energy range is approximate.

Fig. 3.—Overlay of Fregate band C (30–400 keV; *solid line*) and SXC (2–10 keV; *dashed line*) light curves for GRB 030329 showing the distinct nature of the two pulses of GRB 030329. There is a delay of ∼5 s between the peak of the 30–400 keV and 2–10 keV emission in the first pulse, while the two are essentially simultaneous in the second pulse. (The SXC light curve has been scaled for clarity.)

of GRB 030329 will be discussed in more detail in J.-L. Atteia et al. (2004, in preparation).

3.3. *Spectrum*

Because the burst was invalidated in flight, there are no time-tagged photon data from the Fregate instrument available. However, survey spectral data, which consists of 128 spectral bins every 5.2 s, can be used to calculate the burst spectral parameters. The spectrum of the entire burst can be well fitted by a Band function from 2–400 keV, with parameters $\alpha = -1.32 \pm 0.02$, $\beta = -2.44 \pm 0.08$, and $E_{\mathrm{peak}} = 70.2 \pm 2.3$ (errors are 90%); however, in time-resolved spectroscopy these parameters vary significantly during the course of the burst. The burst fluence was $S_\gamma = 1.2 \times 10^{-4}$ ergs cm^{-2} in the 30–400 keV band and $S_X = 6.6 \times 10^{-5}$ ergs cm^{-2} in the 2–30 keV band; the hardness ratio S_X/S_γ is 0.56, which qualifies GRB 030329 as an X-ray–rich burst (Heise et al. 2001). At the measured redshift of 0.1685, the total isotropic energy released was $(1.86 \pm 0.08) \times 10^{52}$ ergs and E_{peak} in the source frame is 82.0 ± 2.6 keV, consistent with the relationship described in Amati et al. (2002). The time-integrated emission properties of GRB 030329 in various energy bands are given in Table 2.

The results of time-resolved spectral analyses are given in Table 3 and plotted in Figure 4. The Fregate and WXM data were fitted jointly, to a Band function when possible and a power-law model when a significant value of Band β could not be calculated. The data show a strong softening of the burst spectrum during the course of the first pulse, followed by a mild rehardening at the onset of the second pulse and a subsequent softening.

Power-law fits to the WXM precursor data reveal that the photon indices of the two bumps are similar, -2.0 ± 0.4. A joint fit of a power-law model to the WXM and Fregate data for both bumps together (from $t = -13$ s to $t = +3$ s) shows a photon index of -2.11 ± 0.09, a 2–25 keV fluence of 1.2×10^{-6} ergs cm^{-2}, and a 30–400 keV fluence of 9.3×10^{-7} ergs cm^{-2}. (Fits of the precursor data to a cutoff power-law [Comptonization] model and a Band function were also performed, but neither resulted in a significant improvement in χ^2.) The power-law fit is quite good (reduced χ^2 of 0.7); the precursor spectra are very clearly nonthermal.

4. SOFT X-RAY EMISSION AND PRECURSOR ACTIVITY

4.1. *Spectral Lag or Soft X-Ray Bump?*

At first glance, the broadband light curves shown in Figure 2 seem to indicate that there is a strong hard-to-soft evolution in the burst emission in the first pulse. However, closer evaluation
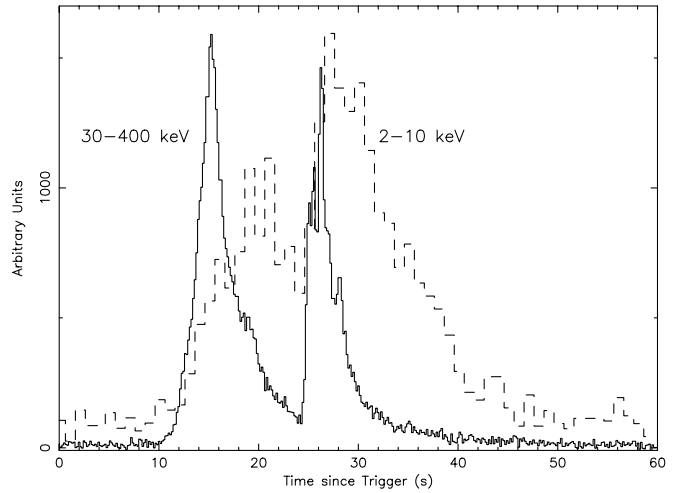
of the burst light curves suggests that this "evolution" is more likely due to a relatively bright, soft X-ray bump of ∼20 s duration centered at $t \approx 20$ s after the burst trigger, as shown in the overlay of band C and SXC emission in Figure 3.

We examined the GRB 030329 burst data for spectral lags of the type discussed in Band (1997). This analysis was made difficult because the Fregate broadband light curve bandpasses do not match up well with the BATSE discriminator bandpasses (20–50 keV, 50–100 keV, 100–300 keV) and because there are no time-tagged photon data with which to reconstruct such light curves; however, linear combinations of Fregate bandpass light curves can be used to shed some light on the spectral evolution of the first pulse of the burst. We calculate the difference of Fregate band B (7–80 keV) and Fregate band A (7–40 keV) to create a Fregate band "B−A" with an effective bandpass of 40–80 keV; we also construct a "C−(B−A)" light curve, which has an effective energy bandpass of 30–40 keV *plus* 80–400 keV. A simple cross-correlation of the band B−A light curve with the band C−(B−A) light curve (160 ms time resolution) shows a "lag" of 6 ± 32 ms. This value indicates that there is essentially no shift in the temporal structure of the GRB 030329 light curve at energies greater than 30 keV, and thus that the strong spectral evolution in the first pulse must be due to photons with $E < 30$ keV.

As an alternate approach to understanding the temporal and spectral variability of the main pulses, we scale the B−A light curve to the C−(B−A) light curve and examine the differences between the two. The scaling is done using only the data at the peak of the first pulse (between $t = 14.5$ and 15.5 s after the trigger); the resulting scale factor is 0.42. In Figure 5 we show the band C−(B−A) light curve, the scaled band B−A light curve, and the difference between the two; the shapes of the light curves match extremely well for the duration of the burst, even though the scaling was done using data only from the maximum of the first pulse. The difference reflects differences in the temporal characteristics of the $(30 - 40) + (80 - 400)$ keV band with respect to the template 40–80 keV band and could be due to features in either the 30–40 keV band or the 80–400 keV band. The difference is consistent with zero except for a few pulse-like features—most notable are a peak at

TABLE 2
EMISSION PROPERTIES OF GRB 030329

Energy (keV)	Photon Flux (photons cm^{-2} s^{-1})	Energy Flux (10^{-7} ergs cm^{-2} s^{-1})	Energy Fluence (10^{-5} ergs cm^{-2})
2–10	57.5 ± 1.1	4.20 ± 0.07	2.64 ± 0.04
2–25	77.0 ± 1.1	9.16 ± 0.08	5.76 ± 0.05
2–30	79.9 ± 1.1	10.43 ± 0.08	6.57 ± 0.05
7–30	32.35 ± 0.19	7.53 ± 0.04	4.74 ± 0.03
30–400	15.09 ± 0.10	18.78 ± 0.25	11.82 ± 0.16
50–100	5.39 ± 0.05	5.98 ± 0.06	3.76 ± 0.04
100–300	2.91 ± 0.05	7.35 ± 0.16	4.62 ± 0.10

NOTE.—Errors are for 90% confidence. All values were calculated from the time-averaged Band spectrum of the entire burst.

$t = 20$ s, consistent with the peak of the soft X-ray emission (Fig. 3), a peak at the start of the second pulse ($t = 25$ s), and a spike coincident with the band D spike ($t = 26$ s)—and a faint tail starting at $t = 28$ s. Interpretation of the details of this difference is not straightforward; however, this analysis confirms that the extreme "lag" implied by the light curves in Figures 2 and 3 is not seen at energies greater than 30 keV.

The more likely explanation for the time profiles seen in Figures 2 and 3 is a bump of soft X-ray emission, which begins at about the same time as the main GRB and peaks at $t \approx 20$ s, 5 s after the peak of the first pulse. Analysis of the 2–10 keV light curve shows that a Gaussian with a FWHM of ∼12 s is a reasonable fit to that pulse; we estimate the 2–10 keV fluence of this pulse to be ∼7×10^{-6} ergs cm^{-2} (because the spectrum of GRB itself extends into the soft X-ray band, it is not possible to clearly separate the first pulse into the sum of two distinct light curves).

Detailed spectral analyses of the soft X-ray pulse are made difficult by the overlap with the first GRB pulse and the absence of high time resolution spectral data; thus it is not possible to demonstrate the existence of the soft X-ray pulse by fitting the spectrum of GRB 030329 to a two-component spectral model. The excellent fit of the burst spectrum to a GRB model (Band et al. 1993) in that time period indicates that the soft pulse likely has a nonthermal spectrum. If the

broadband light curve data are not considered, it would be easy to disregard this soft emission as part of the spectral evolution of the GRB; however, the dissimilarity in the 2–10 keV and band C light curves in the first pulse and the stark contrast in the burst emission profiles above 30 keV versus below 20 keV strongly suggest that the soft X-ray pulse is indeed a distinct emission component.

The behavior of the soft X-rays of the second pulse is entirely different from that of the first pulse. The fast rise of the 2–10 keV count rate in the second pulse is coincident with the onset of the second pulse in the band C light curve, in contrast to the delayed rise of the 2–10 keV component of the first pulse. There is no evidence for a distinct soft X-ray component in the second pulse; the similarity of the band C and 2–25 keV
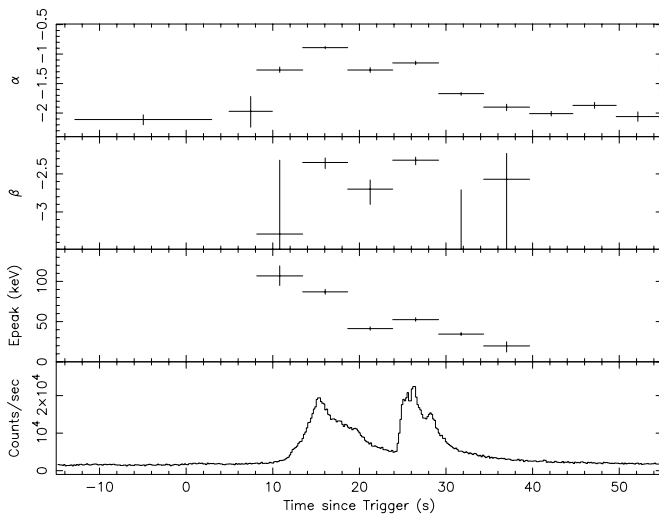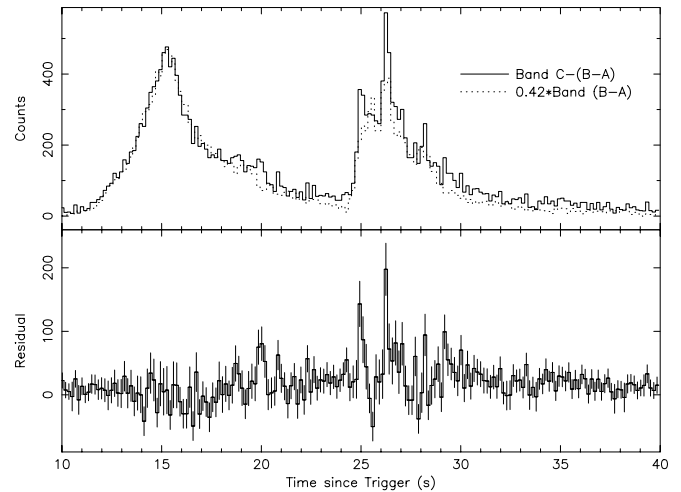

FIG. 5.—GRB 030329 40–80 keV light curve, calculated as Fregate band B minus Fregate band A, scaled to the 30–400 keV minus the 40–80 keV light curve using a 1 s interval centered on the peak of the first pulse ($t = 14.5$ s to $t = 15.5$ s). The 40–80 keV light curve is multiplied by the ratio of the counts fluence in that time period (0.42) and compared to the band C−(B−A) light curve. The two light curves are shown in the top panel; the solid line is band C−(B−A), and the dotted line is 0.42 times band(B−A). The difference between the two (*bottom panel*) reflects excesses in either the 30–40 keV or the 80–300 keV band with respect to the template defined by the B−A light curve. The difference is consistent with zero except for a peak at $t = 20$ s (coincident with the peak of the soft X-ray emission in the first pulse), two short spikes at $t = 25$ s (coincident with the onset of the second pulse) and $t = 26.2$ s (coincident with the spike in band D), and a faint extended tail starting at about $t = 28$ s (consistent with an extended soft tail to the burst). We conclude that the overall shape of the light curve of GRB 030329 does not vary significantly from 30 to 400 keV, and thus that the soft X-ray pulse seen in Fig. 3 could be due to a different emission mechanism than the main burst.

FIG. 4.—Variation of the spectral parameters of GRB 030329 with time. Shown are the Band α, β, and E_{peak} parameters with the band B light curve for reference; for regions where Band β cannot be calculated, α is the index in a fit of a power law to the counts spectrum.

TABLE 3
Spectral Model Parameters for GRB 030329

Time since trigger (s)	α[a]	β	E_{peak} (keV)	2–25 keV Flux (10^{-7} ergs cm^{-2} s^{-1})	30–400 keV Flux (10^{-7} ergs cm^{-2} s^{-1})
-10.05 to -5.05[b]	$-2.16^{+0.38}_{-0.44}$	...	...	$0.66^{+0.18}_{-0.17}$	...
-5.05 to -0.05[b]	$-1.96^{+0.49}_{-0.56}$	...	...	$0.68^{+0.23}_{-0.20}$	...
-0.05 to -4.95[b]	$-2.01^{+0.31}_{-0.30}$	...	...	$1.18^{+0.24}_{-0.20}$	...
4.95 to 9.95[b]	$-1.97^{+0.25}_{-0.27}$	...	...	$1.37^{+0.23}_{-0.22}$	...
-12.85 to -2.95	$-2.11^{+0.08}_{-0.09}$	...	...	$0.77^{+0.07}_{-0.07}$	$0.59^{+0.14}_{-0.12}$
8.15 to -13.45	$-1.27^{+0.05}_{-0.04}$	$-3.29^{+0.97}_{-6.71}$	$106.80^{+12.48}_{-11.94}$	$5.03^{+0.15}_{-0.15}$	$14.12^{+0.72}_{-0.67}$
13.45 to -18.65	$-0.89^{+0.02}_{-0.02}$	$-2.35^{+0.06}_{-0.08}$	$87.03^{+3.16}_{-2.98}$	$24.12^{+0.24}_{-0.26}$	$95.69^{+1.28}_{-1.27}$
18.65 to -23.85	$-1.27^{+0.04}_{-0.04}$	$-2.70^{+0.12}_{-0.20}$	$41.35^{+2.21}_{-2.00}$	$17.57^{+0.25}_{-0.23}$	$22.66^{+0.69}_{-0.73}$
23.85 to -29.15	$-1.15^{+0.03}_{-0.03}$	$-2.32^{+0.04}_{-0.06}$	$52.45^{+2.41}_{-2.00}$	$33.34^{+0.31}_{-0.30}$	$66.74^{+1.04}_{-1.04}$
29.15 to -34.35	$-1.67^{+0.02}_{-0.03}$	$-4.57^{+1.86}_{-5.43}$	$34.45^{+2.00}_{-1.84}$	$14.39^{+0.24}_{-0.24}$	$12.29^{+0.83}_{-0.23}$
34.35 to -39.65	$-1.90^{+0.05}_{-0.06}$	$-2.57^{+0.34}_{-7.43}$	$19.81^{+5.17}_{-7.62}$	$6.38^{+0.19}_{-0.18}$	$4.99^{+0.55}_{-0.62}$
39.65 to -44.65	$-2.01^{+0.04}_{-0.04}$	...	...	$3.47^{+0.15}_{-0.15}$	$3.50^{+0.30}_{-0.29}$
44.65 to -49.65	$-1.87^{+0.05}_{-0.05}$	...	...	$1.95^{+0.12}_{-0.13}$	$2.85^{+0.31}_{-0.31}$
49.65 to -54.65	$-2.06^{+0.08}_{-0.08}$	...	...	$1.50^{+0.13}_{-0.13}$	$1.30^{+0.26}_{-0.23}$
54.65 to -59.65	$-2.14^{+0.11}_{-0.12}$	...	...	$1.17^{+0.13}_{-0.12}$	$0.82^{+0.25}_{-0.22}$
59.65 to -64.65	$-2.36^{+0.14}_{-0.16}$	...	...	$0.93^{+0.12}_{-0.12}$	$0.35^{+0.16}_{-0.12}$

Note.—All errors are for 90% confidence.

[a] Parameter α is the Band α parameter for those time regions where a Band β value is specified; otherwise, it is the index for a simple power-law fit.

[b] Only WXM data were used in the fit.

time profiles in the second pulse indicates that the emission in these two bands likely come from the same source, with any variations in relative brightness being due to spectral parameters changing as a function of time (see Fig. 4).

4.2. *Precursors*

The concept of a burst "precursor" has various definitions when applied to GRBs. The original definitions were ostensibly "γ-rays seen before the pulse that triggered the instrument" or "X-rays seen before the γ-rays." The term "precursor" has been applied to γ-ray pulses before the event that triggered BATSE (Koshut et al. 1995) and to the slow onset of soft X-ray emission before the main γ-ray pulse (e.g., GRB 900623; Murakami et al. 1991), as well as to isolated X-ray pulses before the GRB itself (e.g., GRB 790307; Laros et al. 1984).

Koshut et al. (1995) defined a precursor to be emission that precedes the main burst by at least the duration of the main burst; using this restrictive definition and BATSE DISCLA data with $E > 25$ keV, they found that the distribution of "precursor" spectral parameters is not significantly different from the distribution of GRB spectral parameters. On the other hand, in 't Zand et al. (1999) distinguish precursor emission from the burst emission by *requiring* that the precursor emission be described by an entirely different spectral model than the burst emission or that the spectral parameters of the precursor be unprecedented in describing GRBs in the γ-ray phase. According to in 't Zand et al., then, the thermal emission of GRB 900126 (Murakami et al. 1991) is a true precursor, while the "X-ray bumps before the GRB" in GRB 980519 and GRB 990704 (Feroci et al. 2001) are not. Koshut et al. would not consider any of these examples to be true precursors; however, these precursors are so soft that they would not have been considered in their analysis.

The features in the low-energy light curves of GRB 030329 at $t \approx -10$ s and $t \approx 2$ s are very similar to the "X-ray bumps before the GRB" in GRB 980519. In that burst, detected by *BeppoSAX*, three soft X-ray bumps precede the main burst by 10–40 s, and the bumps are nonthermal and are well fitted by a power law of index ~-2; in 't Zand et al. (1999) consider these bumps to be part of the main burst emission. In fact, the spectral evolution of GRB 980519 overall is quite similar to that of GRB 030329, as the power-law index is ~-1 at the peak of the burst, then settles to values near -2 as the burst fades. GRB 980519 is significantly fainter, however; the 25–300 keV fluence is 7×10^{-6} ergs cm^{-2}, roughly 15 times fainter than GRB 030329. Scaling from Figure 2 of in 't Zand et al. (1999), the 2–10 keV fluence of the "X-ray bumps before the GRB" of GRB 980519 is $\sim 5 \times 10^{-7}$ ergs cm^{-2}, which, for a power law of index -2, is comparable to the 2–25 keV fluence of $\sim 10^{-6}$ ergs cm^{-2} for GRB 030329. It is unclear whether the fact that these pre-GRB X-ray fluences are so similar for bursts that differ by more than 10 times in overall fluence is an indication that an independent mechanism is responsible for the creation of the pre-GRB X-rays; the detection of more bursts of this kind is required to understand this better. Several bursts in the *HETE* database have similar X-ray "precursors"; these will be discussed in a separate paper.

5. CONCLUSIONS

GRB 030329 was seen as a two-peaked GRB with $S_\gamma = 1.2 \times 10^{-4}$ ergs cm^{-2}, making it the brightest GRB detected by *HETE* and one of the brightest GRBs ever detected. The substantial X-ray fluence of GRB 030329 (6.6×10^{-5} ergs cm^{-2}) puts it in the class of X-ray–rich GRBs. The overall burst can be fitted well with a GRB model, with $\alpha = -1.32 \pm 0.02$, $\beta = -2.44 \pm .08$, and $E_{\text{peak}} = 70.2 \pm 2.3$ keV, but there is substantial spectral variability during the burst.

Detailed analyses of the burst light curves reveal the presence of a soft X-ray component distinct from the main GRB. This component consists almost entirely of photons with energies greater than 25 keV and is quite bright; the 2–10 keV fluence is $\sim 7 \times 10^{-6}$ ergs cm^{-2}. The burst light curves also show two soft, nonthermal X-ray "precursor" bumps; while such pre–γ-ray peak X-ray emission has been detected in some GRBs, it is not a common feature of GRB light curves.

The enormous brightness of the optical afterglow of GRB 030329 has allowed it to be used as a "Rosetta Stone" in understanding the correlation of GRBs with Type Ic supernovae. The analysis of the bright prompt X- and γ-ray emission of GRB 030329 has revealed a bright, soft X-ray component apparently uncorrelated with the main body of the burst emission. The obvious presence of this feature in a burst as bright as GRB 030329 leads to the question of whether this feature is present in other GRBs and whether the brightness of the feature scales with burst fluence. This underlying soft pulse would not have been detected by the BATSE LADs, as detectors sensitive to photons with $E < 20$ keV are required to detect these pulses; however, at certain gain settings the BATSE SDs would have detected the soft emission of such an intense event (Preece et al. 2000). Searches for such features in GRBs detected by *HETE* are underway; we urge that similar analyses of *BeppoSAX*, *Ginga*, and BATSE SD data be performed. In this way, perhaps GRB 030329 will also act as a "Rosetta Stone" in furthering our understanding of the prompt X- and γ-ray emission in long GRBs.

REFERENCES

Amati, L., et al. 2002, A&A, 390, 81

Atteia, J.-L., et al. 2003, in AIP Conf. Proc. 662, Gamma-Ray Burst and Afterglow Astronomy 2001, ed. G. R. Ricker & R. K. Vanderspek (New York: AIP), 17

Band, D. 1997, ApJ, 486, 928

Band, D., et al. 1993, ApJ, 413, 281

Berger, E., Soderberg, A. M., & Frail, D. A. 2003, GCN Circ. 2014, http://gcn.gsfc.nasa.gov/gcn/gcn3/2014.gcn3

Burenin, R., et al. 2003, GCN Circ. 2001, http://gcn.gsfc.nasa.gov/gcn/gcn3/2001.gcn3

Crew, G. B., Villasenor, J., Monnelly, G., Doty, J., Vanderspek, R., & Ricker, G. 2003, in AIP Conf. Proc. 662, Gamma-Ray Burst and Afterglow Astronomy 2001, ed. G. R. Ricker & R. K. Vanderspek (New York: AIP), 66

Fenimore, E. E., in 't Zand, J. J. M., Norris, J. P., Bonnell, J. T., & Nemiroff, R. J. 1995, ApJ, 448, L101

Feroci, M., et al. 2001, A&A, 378, 441

Finkelstein, A. M., Ipatov, A. V., & Gnedin, Y. N. 2003, GCN Circ. 2161, http://gcn.gsfc.nasa.gov/gcn/gcn3/2161.gcn3

Gal-Yam, A., Ofek, E. O., Polishook, D., & Leibowitz, E. M. 2003, GCN Circ. 1999, http://gcn.gsfc.nasa.gov/gcn/gcn3/1999.gcn3

Greiner, J., Peimbert, M., Estaban, C., Kaufer, A., Jaunsen, A., Smoke, J., Klose, S., & Reimer, O. 2003, GCN Circ. 2020, http://gcn.gsfc.nasa.gov/gcn/gcn3/2003.gcn3

Heise, J., in 't Zand, J., Kippen, R. M., & Woods, P. 2001, in Gamma-Ray Bursts in the Afterglow Era, ed. E. Costa, F. Frontera, & J. Hjorth (Berlin: Springer), 16

Hjorth, J., et al. 2003, Nature, 423, 847

Hoge, J. C., Meijerink, R., Tilanus, R. P. J., & Smith, I. A. 2003, GCN Circ. 2088, http://gcn.gsfc.nasa.gov/gcn/gcn3/2088.gcn3

in 't Zand, J. J. M., Heise, J., van Paradijs, J., & Fenimore, E. E. 1999, ApJ, 516, L57

Klose, S., Hoegner, C., & Greiner, J. 2003, GCN Circ. 2000, http://gcn.gsfc.nasa.gov/gcn/gcn3/2000.gcn3

Koshut, T. M., Kouveliotou, C., Paciesas, W. S., van Paradijs, J., Pendleton, G. N., Briggs, M. S., Fishman, G. J., & Meegan, C. A. 1995, ApJ, 452, 145

Kouveliotou, C., Meegan, C. A., Fishman, G. J., Bhat, N. P., Briggs, M. S., Koshut, T. M., Paciesas, W. S., & Pendleton, G. N. 1993, ApJ, 413, L101

Kuno, N., Sato, N., & Nakanishi, H. 2003, GCN Circ. 2089, http://gcn.gsfc.nasa.gov/gcn/gcn3/2089.gcn3

Laros, J. G., Evans, W. D., Fenimore, E. E., Klebesadel, R. W., Shulman, S., & Fritz, G. 1984, ApJ, 286, 681

Lidman, C., et al. 1998, IAU Circ. 6895, 2, http://cfa-www.harvard.edu/iauc/06800/06895.html

Lipunov, V., et al. 2003, GCN Circ. 2002, http://gcn.gsfc.nasa.gov/gcn/gcn3/2002.gcn3

MacFadyen, A., & Woosley, S. E. 1999, ApJ, 524, 262

Marshall, F. E., Markwardt, C., & Swank, J. H. 2003, GCN Circ. 2052, http://gcn.gsfc.nasa.gov/gcn/gcn3/2052.gcn3

Marshall, F. E., & Swank, J. H. 2003, GCN Circ. 1996, http://gcn.gsfc.nasa.gov/gcn/gcn3/1996.gcn3

Matheson, T., et al. 2003, GCN Circ. 2107, http://gcn.gsfc.nasa.gov/gcn/gcn3/2107.gcn3

Murakami, T., Inoue, H., Nishimura, J., van Paradijs, J., & Fenimore, E. E. 1991, Nature, 350, 592

Peterson, B. A., & Price, P. A. 2003, GCN Circ. 1985, http://gcn.gsfc.nasa.gov/gcn/gcn3/1985.gcn3

Pooley, G. 2003, GCN Circ. 2043, http://gcn.gsfc.nasa.gov/gcn/gcn3/2043.gcn3

Pramesh Rao, A., Ishwara-Chandra, C. H., & Bhattacharya, D. 2003, GCN Circ. 2073, http://gcn.gsfc.nasa.gov/gcn/gcn3/2073.gcn3

Preece, R. D., Briggs, M. S., Mallozzi, R. S., Pendleton, G. N., Paciesas, W. S., & Band, D. L. 2000, ApJS, 126, 19

Price, P. A., et al. 2003, Nature, 423, 844

Prochaska, J. X., Bloom, J. S., Chen, H. W., Hurley, K., Dressler, A., & Osip, D. 2003, GCN Circ. 2482, http://gcn.gsfc.nasa.gov/gcn/gcn3/2482.gcn3

Ricker, G. R., et al. 2003, in AIP Conf. Proc. 662, Gamma-Ray Burst and Afterglow Astronomy 2001, ed. G. R. Ricker & R. K. Vanderspek (New York: AIP), 3

Schnoor, P. W., Welch, D. L., Fishman, G. J., & Price, A. 2003, GCN Circ. 2176, http://gcn.gsfc.nasa.gov/gcn/gcn3/2176.gcn3

Shirasaki, Y., et al. 2003, PASJ, 55, 1033

Smith, D. A., et al. 2003, ApJ, 596, L151

Stanek, K. Z., et al. 2003, ApJ, 591, L17

Tiengo, A., Mereghetti, S., Ghisellini, G., Rossi, E., Ghirlanda, G., & Schartel, N. 2003, A&A, 409, 983

Tinney, C., Stathakis, R., & Cannon, R. 1998, IAU Circ. 6896, http://cfa-www.harvard.edu/iauc/06800/06896.html

Torii, K. 2003, GCN Circ. 1986, http://gcn.gsfc.nasa.gov/gcn/gcn3/1986.gcn3

Uemura, M. 2003, GCN Circ. 1989, http://gcn.gsfc.nasa.gov/gcn/gcn3/1989.gcn3

Vanderspek, R., et al. 2003, GCN Circ. 1997, http://gcn.gsfc.nasa.gov/gcn/gcn3/1997.gcn3

Villasenor, J. N., et al. 2003, in AIP Conf. Proc. 662, Gamma-Ray Burst and Afterglow Astronomy 2001, ed. G. R. Ricker & R. K. Vanderspek (New York: AIP), 33

Watson, D., et al. 2004, ApJ, 605, L101

Woosley, S. E. 1993, ApJ, 405, 273